

Article

# Investigation of Ash Deposition Dynamic Process in an Industrial Biomass CFB Boiler Burning High-Alkali and Low-Chlorine Fuel

Hengli Zhang, Chunjiang Yu, Zhongyang Luo \*  and Yu'an Li

State Key Laboratory of Clean Energy Utilization, Zhejiang University, Hangzhou 310027, China; hlzhang@zju.edu.cn (H.Z.); chunjiang@zju.edu.cn (C.Y.); lyua@zju.edu.cn (Y.L.)

\* Correspondence: zyluo@zju.edu.cn; Tel.: +86-571-8795-2440

Received: 17 January 2020; Accepted: 26 February 2020; Published: 2 March 2020



**Abstract:** The circulating fluidized bed (CFB) boiler is a mainstream technology of biomass combustion generation in China. The high flue gas flow rate and relatively low combustion temperature of CFB make the deposition process different from that of a grate furnace. The dynamic deposition process of biomass ash needs further research, especially in industrial CFB boilers. In this study, a temperature-controlled ash deposit probe was used to sample the deposits in a 12 MW CFB boiler. Through the analysis of multiple deposit samples with different deposition times, the changes in micromorphology and chemical composition of the deposits in each deposition stage can be observed more distinctively. The initial deposits mainly consist of particles smaller than 2  $\mu\text{m}$ , caused by thermophoretic deposition. The second stage is the condensation of alkali metal. Different from the condensation of KCl reported by most previous literatures, KOH is found in deposits in place of KCl. Then, it reacts with  $\text{SO}_2$ ,  $\text{O}_2$  and  $\text{H}_2\text{O}$  to form  $\text{K}_2\text{SO}_4$ . In the third stage, the higher outer layer temperature of deposits reduces the condensation rate of KOH significantly. Meanwhile, the rougher surface of deposits allowed more calcium salts in fly ash to deposit through inertial impact. Thus, the elemental composition of deposits surface shows an overall trend of K decreasing and Ca increasing.

**Keywords:** deposit; biomass industrial boiler; alkali metal; circulating fluidized bed

## 1. Introduction

Compared with fossil energy, biomass has the characteristics of zero  $\text{CO}_2$  emission. Biomass direct combustion technology for power generation, as a relatively mature large-scale biomass utilization technology, has been widely used in China. Biomass power generation in China mainly adopts grate furnaces and circulating fluidized bed (CFB) boilers [1]. CFB boilers have a wide combustion adaptability, low combustion temperature and good gas–solid mixing characteristics in the bed, making them a very suitable combustion technology for biomass. This technology has taken up a large proportion in biomass power generation projects in recent years in China [1]. The dominant elements in biomass ash are Ca, K, Cl and S [2,3]. During combustion, K element in biomass fuel is released to the gas phase in the form of KCl, KOH and  $\text{K}_2\text{SO}_4$  [4–10]. These potassium-containing compounds cause severe slagging due to their low melting temperature [11–16].

The study of deposition on the heating surface of biomass power plants is mostly carried out by analyzing mature deposits sampled in boiler maintenance. The innermost layer of deposits typically contains iron oxide, KCl, and  $\text{K}_2\text{SO}_4$ . The intermediate layer contains melt KCl and other ash particle [1,12,13,17–19]. In some deposits, an in situ reaction between KCl and the captured ash particles will occur, leading to the release of chlorine-containing gases. But, through the analysis of

mature deposits, the dynamic deposition process is difficult to study clearly and in detail. On the one hand, the long-term deposition process makes the deposit undergo a chemical reaction and changes its morphology and chemical composition, compared to its initial state when the deposit formed. On the other hand, the mature deposit derived from biomass ash is tight and hard, making it difficult to stratify in order to analyze and study the deposition process, especially the extremely thin deposit layer at the initial deposition stage.

To avoid the disadvantages of mature deposits, an ash deposition probe has been used to “real-time” sample the deposits in some of the literature. Some research works focused on the deposit formation rate and studied the influences of the probe surface temperature, flue gas temperature, fuel type (alkali metal content), probe exposure time and additives on the deposit formation rate [20–22]. Others used the deposition probe to get short-term deposits to analyze the deposition mechanism [23]. In addition, an ash deposition probe was also used to measure corrosion rate caused by alkali metal deposits at different flue gas temperatures and probe surface temperatures on three types of superheater steel [24–26]. These literatures focused more on the deposit formation rate and the corrosion rate. Although some investigation of the deposition mechanism using an ash deposition probe has been carried out, the analysis was based on one deposit sample, resulting in an unclear dynamic deposition process.

In this work, the deposit build-up process on an ash deposition probe at different deposition times is studied. Through the analysis of multiple deposits samples with different deposition times, the dynamic deposition process was shown more clearly and in detail. In addition, this work is carried out in a full-scale 12 MW biomass CFB boiler, enriching the previous studies in the field of biomass CFB boiler ash deposition, especially industrial CFB boilers.

## 2. Materials and Methods

### 2.1. MW Biomass CFB Boiler

In order to study the mechanism of deposition on a high-temperature superheater of a CFB boiler burning biomass with high-alkali metal content, the experiment was carried out in a CFB boiler at a biomass power plant (2 × 12 MW) in Jiangsu province, China. The boiler operates at a medium temperature and pressure (main steam parameters are 450 °C, 3.82 MPa.), and has the capacity of 75 tons/h. Deposition occurred during the operation process.

The 12 MW medium temperature and medium pressure CFB boiler of a biomass power plant adopts the low-temperature fluidized combustion scheme of Zhejiang University. A sketch is given in Figure 1. Through combustion organization and boiler design, the temperature of different regions in the furnace is well controlled, effectively inhibiting the alkali metal problem in the combustion process of high-alkali biomass fuel. This scheme makes use of the characteristics of high combustion activity and low burnout temperature of biomass semi-coke to control the temperature of the boiler dense phase area and return loop at 750 °C or lower, thus eliminating the bed material agglomeration or slagging in the dense phase area and return material loop. Through the arrangement of the heating surface and the control of the circulation ratio, the central volatile combustion area temperature is controlled under 820 °C, minimizing the migration of alkali metals into the gas phase, thus inhibiting deposition and high-temperature corrosion on the heating surface. This scheme has been successfully applied in a large number of engineering practices, significantly inhibiting various alkali metal problems on the basis of ensuring combustion efficiency.

Nevertheless, ash deposition on the heat transfer surface of ZJU CFB boiler has been also found, which is a hard and thick deposit on the superheater.

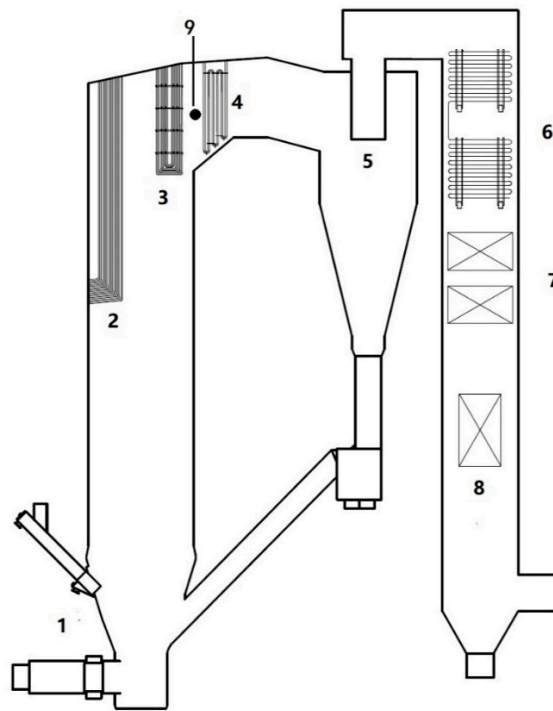


**Figure 1.** The 12 MW biomass circulating fluidized bed (CFB) boiler: 1. feeder; 2. water wall; 3. platen superheater; 4. high-temperature superheater; 5. cyclone separator; 6. low-temperature superheater; 7. economizer; 8. air preheater; 9. location of deposition probe.

## 2.2. Fuel

The blended biomass fuel consisted of rice husks (30%), bark (30%), construction plywood wastes (30%) and other biomass fuels such as lees of wine (10%). The industrial analysis, heating value and elemental analysis of the blended fuel are shown in Table 1. K was analyzed by atomic absorption spectroscopy (AAS) after microwave digestion, while Cl and  $\text{SO}_4^{2-}$  were analyzed by ion chromatography. Compared to typical straw biomass, this blended biomass fuel had a similar K content and much lower Cl content, which may have affected the migration of alkali metal (K) during combustion and deposition characteristic.

**Table 1.** Physicochemical properties of blended biomass fuel.

Item	Symbol	Blended Biomass Fuel
Proximate analysis	moisture (% ad)	7.66
	ash (% ad)	5.04
	volatile (% ad)	69.4
	fixed carbon (% ad)	17.9
Ultimate analysis	C (% ad)	43.78
	H (% ad)	4.59
	N (% ad)	1.35
	S (% ad)	0.09
Heating value	O (% ad)	37.49
	Q (kJ/kg, ad)	18312
Inorganic constituent (dry basis)	K (%)	0.41
	$\text{SO}_4^{2-}$ (%)	0.45
	Cl (%)	0.09

X-ray diffraction (XRD) and energy spectrum (EDS) results of fly ash are shown in Figure 2 and Table 2. The high contents of K and  $\text{SO}_4^{2-}$  are also reflected in the composition of fly ash. The main

components of fly ash are identified as  $\text{CaSO}_4$ ,  $\text{CaCO}_3$ ,  $\text{SiO}_2$  and  $\text{K}_2\text{Ca}(\text{SO}_4)_2 \cdot \text{H}_2\text{O}$ .  $\text{SiO}_2$  comes from biomass or bed material. Due to the low content of other components and the complexity of ash composition, no other obvious diffraction peaks are found in the XRD diagram.

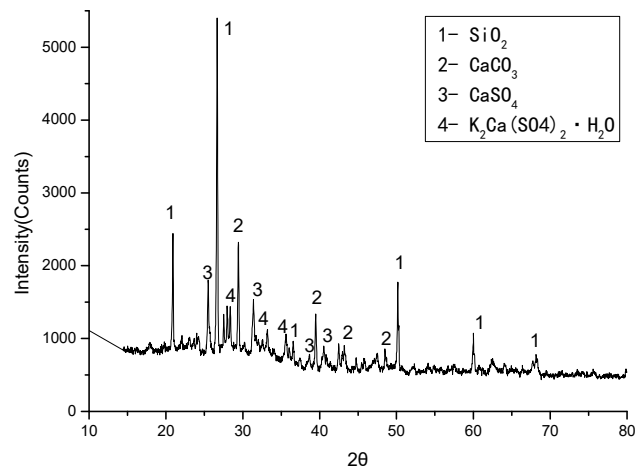


Figure 2. XRD result of fly ash.

Table 2. Elemental composition of fly ash.

	C	O	Na	Mg	Al	Si	P	S	Cl	K	Ca	Fe
Fly ash	16.61	30.91	1.30	2.05	5.38	9.72	0.72	2.40	0.87	7.37	19.26	3.40

### 2.3. Collection and Analysis of Deposits

A temperature-controlled deposit probe was used to sample deposits inside the boiler in this study, set in the high temperature superheater region through a reserved hole prepared for the boiler soot blowing system, shown in Figure 3. Through the analysis of the deposit surface microstructure and elemental distributions with different sampling time intervals, this study studied the dynamic process of deposition.

The normal operation of the boiler combustion temperature is between 750 and 800 °C, while the flue gas temperature in the high temperature superheater inlet is about 700 °C. A sketch of the ash deposit probe is shown in Figure 4. The whole system included a fan, an electric control valve, a digital display controller, a thermocouple and a stainless-steel probe. The probe was about 2.5 m in length with an outer diameter of 38 mm. A thin endless stainless-steel belt was attached to the probe, which was used to sample the ash deposits. In order to keep the same surface conditions as the high temperature superheater, the probe was cooled by air to keep a stable temperature of the sampling belt surface, with a K-type thermocouple testing its temperature. Considering the main steam temperature of the boiler (450 °C) and the flue gas temperature in the high temperature-superheater region (700 °C), the surface temperature of the high-temperature superheater was estimated to be around 500 °C. So, the stable endless stainless-steel belt surface temperature was set at 500 °C.

The sampling tests lasted 1, 2, 5, 15, 24, and 48 h. In each test, we used a new sampling belt to attach to the probe. After the deposits were captured on the sampling belt, the sample, along with the sampling belt, were analyzed directly by SEM-EDS. The micromorphology of ash deposits was observed with SEM. Simultaneously, the element contents of the microstructure observed were measured by EDS. Considering that EDS analysis has a relatively large testing error for element O and C, all the EDS results of deposits given below removed the data of O and C, then were normalized again. Through the experiment and analysis mentioned above, dynamic deposition experiment can conduct the dynamic collection of ash accumulation at each stage of deposition, and observe the changes in morphology and chemical composition more intuitively at the initial stage of deposition.

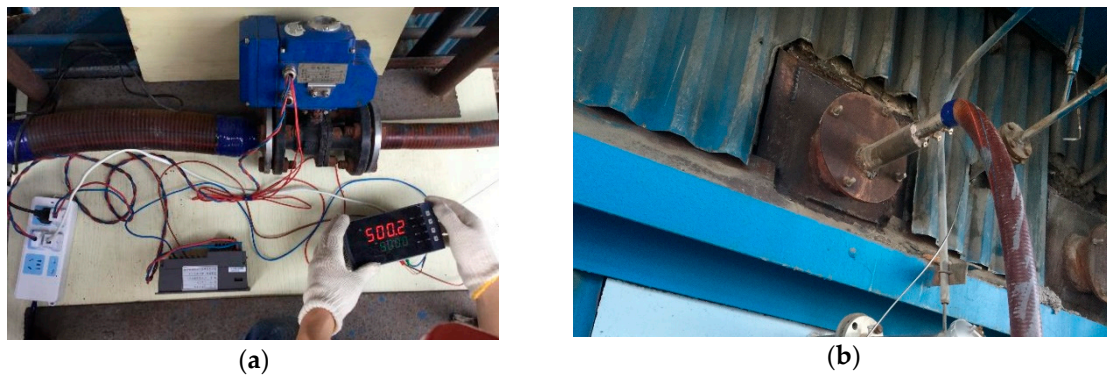


**Figure 3.** Temperature-controlled deposit probe system. (a) Temperature controlling system; (b) The deposit probe.

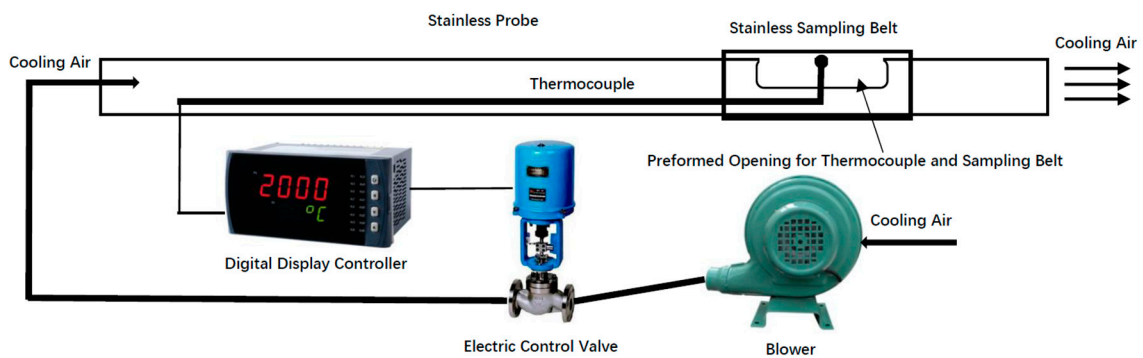


**Figure 4.** Sketch of temperature-controlled ash deposit probe.

### 3. Results and Discussion

Photos of the deposit sampling belt are shown in Figure 5. Within the first 5 h of deposition, the surface is shiny and dark gray. After 15 h, the khaki deposits began to accumulate. The deposit sampling belt is heated to 500 °C in muffle furnace in air as a control sample (Figure 6). The surface is smooth, except some fine particles, which are supposed to be caused by dust in the muffle furnace.

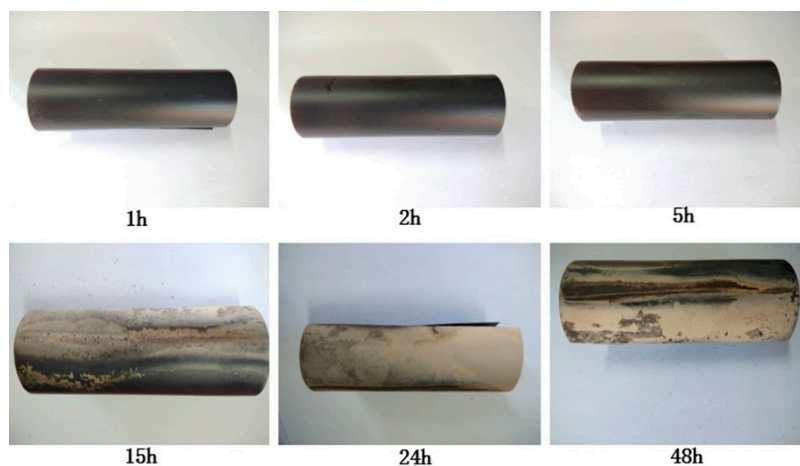


**Figure 5.** Sampling belt at different deposition times.

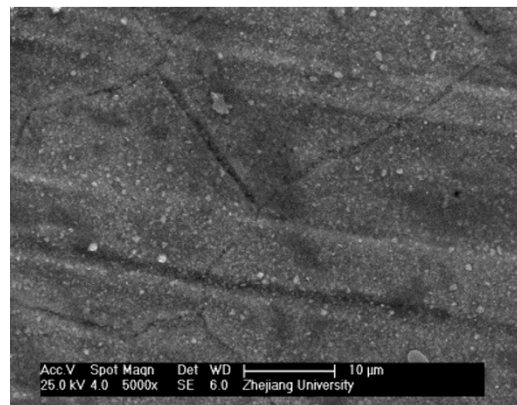


**Figure 6.** The surface of original sampling belt.

### 3.1. Initial Deposition

In the period of initial deposition (samples of 1 h deposits and 2 h deposits), the main contents of metal elements are Ca and Mg. On the contrary, the content of K is very low, with only 3.34% (1 h) and 2.44% (2 h), respectively, as shown in Table 3, which is very different to the viewpoint that initial deposition is caused by alkali salt, as argued in some studies [12,13,17–19]. The surface microstructure under SEM is shown in Figure 7. The deposits consist of particles less than 1 μm in diameter. According to deposition theory, the deposition of particles in this size is dominated by thermoplastic forces, moving from the high-temperature towards the low-temperature area, captured by the heating surface.

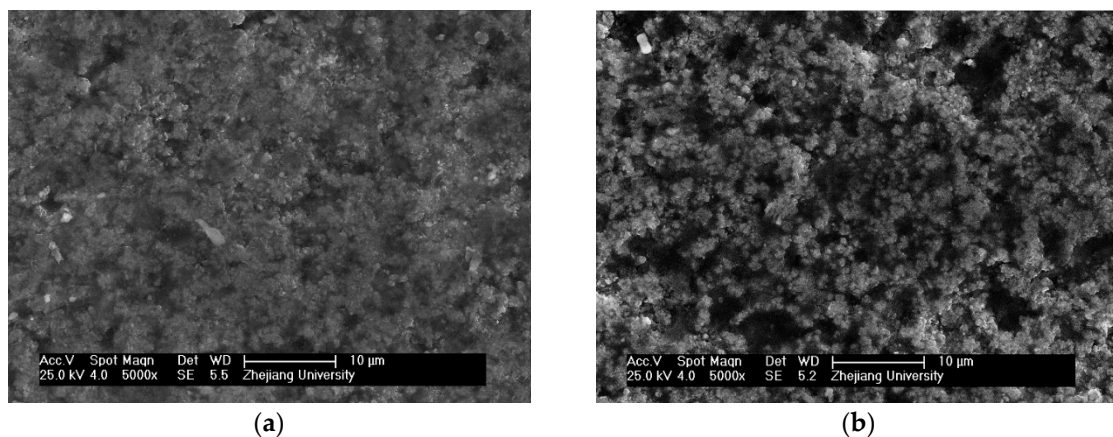


**Figure 7.** Deposits after 1 and 2 h under 5000 times magnified SEM field. (a) Deposits after 1 h; (b) Deposits after 2 h.

**Table 3.** Elemental composition of 1, 2 h deposits and fly ash particles less than 2 μm.

Element	Na	Mg	Al	Si	P	S	Cl	K	Ca
Deposits of 1 h	4.35	15.46	4.56	12.16	5.37	19.93	2.85	3.34	32.02
Deposits of 2 h	1.83	16.18	4.58	11.84	5.26	18.25	1.83	2.44	37.79
Fly ash < 2 μm	2.27	18.01	4.37	12.11	5.13	19.09	1.51	2.09	35.41

### 3.2. Migration and Deposition of Alkali Metal

The deposits after 5 and 15 h show a significantly different microstructure from the previous two deposit samples. The deposit particles become larger, as shown in Figure 8. The EDS analysis (Table 4) of the whole SEM field shows that the main elements are Ca, S, Si and K. Compared to the deposits after 1 and 2h, the content of K begins to rise, but the remarkable presence of Cl is still not detected, proving that alkali does not exist in form of KCl. The large smooth crystalline particles in Spot 1 and 2

are measured by EDS separately, and the results are also shown in Table 4. Their main elements are K, Ca, S. Converting mass to atomic ratio, the atomic number of K, Ca and S conforms to the relation  $(K/2 + Ca) = S$ . It is speculated that the smooth crystalline particles in the field of SEM are a mixture or compound salt of  $CaSO_4$  and  $K_2SO_4$ . Similar crystalline particles in other SEM fields were also selected for EDS analysis, and similar results were obtained.

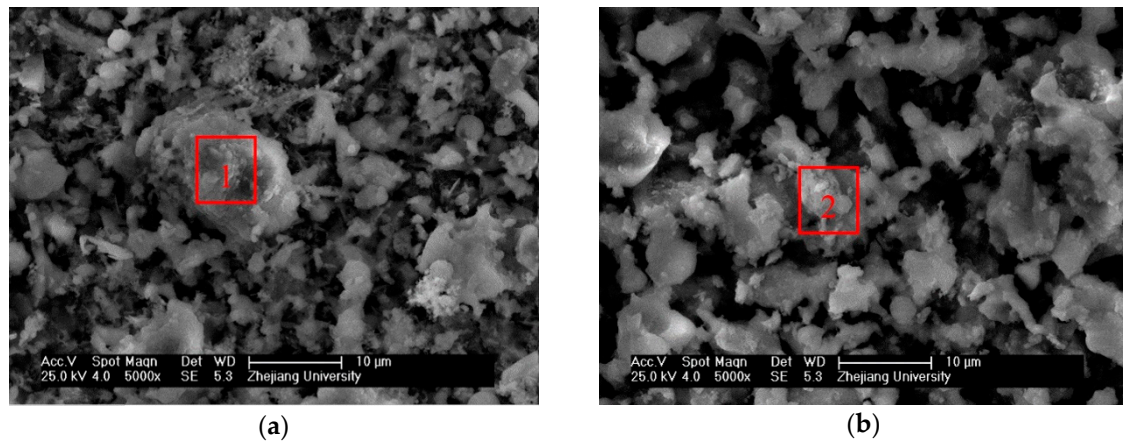


**Figure 8.** Deposits after 5 and 15 h under 5000 times magnified SEM field. (a) Deposits after 5 h; (b) Deposits after 15 h.

**Table 4.** Elemental composition of 5 h and 15 h deposits.

Element	Na	Mg	Al	Si	P	S	Cl	K	Ca
5 h	3.97	5.80	4.06	15.14	1.11	26.32	0.00	22.84	20.75
15 h	4.66	3.87	3.34	9.78	1.46	25.20	0.25	34.36	17.07
Spot 1	1.18	1.08	1.25	2.84	1.08	34.91	0.57	27.59	29.46
Spot 2	1.92	1.11	1.21	2.97	0.56	34.85	0.00	31.25	26.10

According to the K migration mechanism, during the process of combustion, K will release into the gas phase in the form of KCl, KOH and  $K_2SO_4$ , depending on the combustion temperature and fuel characteristics. In this study, with the condition of combustion temperature (800 °C),  $K_2SO_4$  exists in a solid state in fly ash after combustion and will not release into the gas phase. However, the enrichment of potassium salt ( $K_2SO_4$ ) in deposits is much higher than potassium content in fly ash, which is almost impossible directly formed as it is from the fly ash particles' inertial impact. Meanwhile, the potassium salt in deposits of 5 and 15 h have a pure crystalline structure and distribute continuously in the whole visual field of SEM, also indicating that the salt may experience condensation, melting or a chemical reaction rather than direct deposition from fly ash solid particles.

A large number of studies have indicated that the main source of element K in heating surface deposits is gas phase K in biomass combustion [4,5,8–10]. In this study, with the condition of combustion temperature (800 °C) and low Cl content in fuel, K probably enters the gas phase mainly in the form of KOH in place of KCl and  $K_2SO_4$ . Also, in the daily operation of this power plant, the moisture of the blend is up to 30%, enhancing the dissociation reaction to form KOH during combustion with the help of water vapor [8]. Further testing of potassium species in deposits is required. Due to the detection limit of complex mixtures of XRD analysis, minority constituents of the deposits cannot be clearly detected. So, the water-soluble parts of the deposits were selected to be further tested. Deposits after 15 h were dissolved in water and filtered the insoluble matter. Then, the solution was heated and evaporated in order to crystallize to conduct the XRD analysis. The result is shown in Figure 9. Without the interference of the complex insoluble part, the XRD result shows more details. Except for  $K_2SO_4$  and  $CaSO_4$ , which have already been found in SEM-EDS analysis, weak diffraction peaks of

KOH and  $\text{Na}_2\text{SO}_4$  are also found in the water-soluble part of deposits. This indicates that the source of  $\text{K}_2\text{SO}_4$  in deposits is probably KOH.

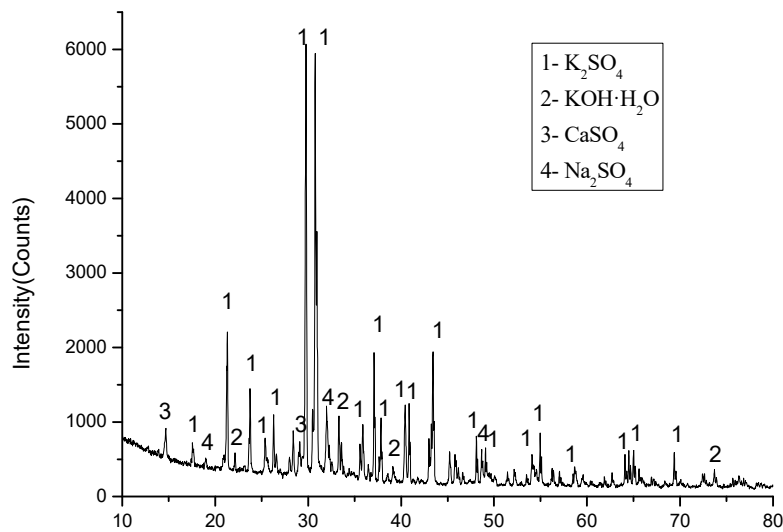


Figure 9. XRD result of water-soluble part of the 15 h deposits.

At this deposition stage, the main deposition process is as follows: during biomass combustion, under a relatively low combustion temperature, low Cl and high moisture content in biomass fuel, element K releases into the gas phase mainly in the form of KOH. Cooled by the high-temperature superheater, KOH condenses on the deposit's surface, and then reacts with  $\text{SO}_2$ ,  $\text{O}_2$  and  $\text{H}_2\text{O}$ , turning KOH into  $\text{K}_2\text{SO}_4$ . Both condensation and the reaction cause  $\text{K}_2\text{SO}_4$  to form a pure crystalline structure and distribute continuously.

It is worth noting that the condensation of KOH and thermophoretic deposition of fine particles in fly ash happen at the same time, all caused by the temperature gradient. In deposition times of 1 and 2 h, thermophoretic deposition rate is higher than the condensation of KOH, becoming the dominant deposition method and leading to high Mg and Ca content and low K content. On the contrary, in deposition times of 5 and 15 h, condensation rate of KOH may be sped up by the rough deposit surface, which provides a condensation nucleus for gas phase KOH. As a consequence, compared to 1 and 2 h, the relative content of K in the 5 and 15 h deposition increased, while the content of Ca decreased, leading to different deposit surface microstructures.

### 3.3. Development of Deposition

When the deposition time reaches 24 and 48 h, the deposits becomes more and more dense. A continuous crystalline structure in Figure 10 (Spot 3 and 4) is still the main deposit component. In terms of K, Ca and S atomic number ratio, this structure is still a mixture or compound salt of  $\text{CaSO}_4$  and  $\text{K}_2\text{SO}_4$ . EDS analysis (Table 5) of the whole SEM visual field shows that K, Ca and S element are not in conformity with the relation of  $(\text{K}/2 + \text{Ca}) = \text{S}$ , but  $(\text{K}/2 + \text{Ca}) > \text{S}$ . This suggests that there are other potassium or calcium slats apart from  $\text{K}_2\text{SO}_4$  and  $\text{CaSO}_4$ . The deposit surface is very rough, providing conditions for the formation of deposits by the inertial impact of fly ash. Combining the XRD result of fly ash shown in Figure 2,  $\text{CaCO}_3$  is likely to be present in these deposits.

Comparing the K and Ca content in 15, 24 and 48 h deposits, a significant decrease occurs in K content, while Ca shows an increasing trend. This is caused by the change in condensation rate of KOH and inertial impact deposition rate. With the development of deposits, the deposition layer becomes thicker, and the surface temperature increases. The temperature gradient between flue gas and deposits surface decreases, reducing the condensation rate of KOH. In contrast, the rough surface

allowed more Ca salts in fly ash to deposit through inertial impact. Thus, the deposits show an overall trend of K decreasing and Ca increasing.

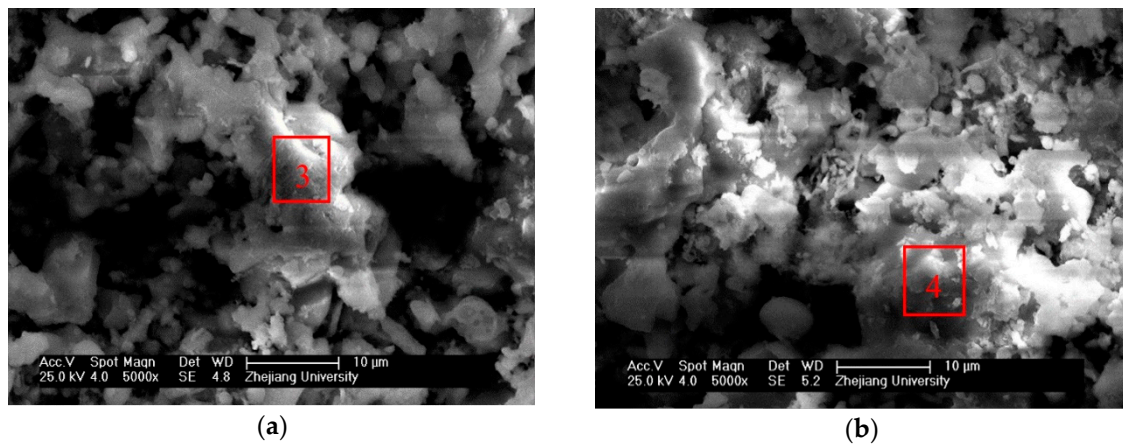


**Figure 10.** Deposits after 24 and 48 h under 5000 times magnified SEM field. (a) Deposits after 24 h; (b) Deposits after 48 h.

**Table 5.** Elemental composition of 24 h and 48 h deposits.

Element	Na	Mg	Al	Si	P	S	Cl	K	Ca
24 h	1.53	3.72	1.81	7.49	1.03	28.72	0.00	26.18	29.54
48 h	1.25	5.48	1.97	9.47	1.15	25.49	0.00	20.58	34.62
Spot 3	0.45	1.61	0.46	1.17	0.41	37.28	0.00	28.99	29.62
Spot 4	0.75	1.00	0.42	1.69	0.42	37.14	0.07	28.19	30.29

#### 4. Conclusions

The dynamic process of ash deposition on the high-temperature superheater of a 12 MW biomass CFB boiler was studied. A temperature-controlled deposit sampling system was used to sample deposit samples with different deposition times. Combustion temperature and inorganic elements in biomass fuel significantly impact the formation of deposits. The deposition process of burning low Cl content biomass fuel is different from that of high Cl content biomass in CFB boiler. Almost no KCl was found in deposits. K exists in the form of  $K_2SO_4$ , which is derived by the reaction of KOH,  $O_2$ ,  $H_2O$  and  $SO_2$ . The deposition process can be identified as three stages:

1. Initial deposition, In the initial stage, the temperature gradient leads to the deposition of fine particles from the flue gas through thermophoretic deposition.
2. Condensation of KOH, Under the condition of a relatively low combustion temperature, low Cl content and high moisture content, K in biomass fuel will release into the gas phase mainly in the form of KOH. In the second stage, after the initial deposition, the surface becomes rough, leading to an acceleration of gas phase KOH condensation on the deposits surface. Then, KOH reacts with  $H_2O$ ,  $O_2$  and  $SO_2$  in flue gas to form the enrichment of  $K_2SO_4$  in deposits.
3. Inertial impact of fly ash, In the third stage, the rougher surface allows fly ash to deposit through inertial impact. At the same time, with the thickening of the deposition layer, the outer layer temperature increases, leading to a significant reduction in KOH condensation rate. Thus, the elemental composition of the deposit's surface shows an overall trend of K decreasing and Ca increasing.

**Author Contributions:** Conceptualization, C.Y. and Z.L.; Investigation, H.Z. and Y.L.; Methodology, H.Z. and C.Y.; Supervision, Z.L.; Writing – original draft, H.Z.; Writing – review & editing, H.Z. and Z.L. All authors have read and agreed to the published version of the manuscript.

**Funding:** This research was funded by International Cooperation Foundation for China-USA, NSFC-NSF 51661125012.

**Conflicts of Interest:** The authors declare no conflict of interest.

## References

1. Li, L.; Yu, C.; Huang, F.; Bai, J.; Fang, M.; Luo, Z. Study on the deposits derived from a biomass circulating fluidized-bed boiler. *Energy Fuels* **2012**, *26*, 6008–6014. [[CrossRef](#)]
2. Zajac, G.; Szyszlak-Barglowicz, J.; Golebiowski, W.; Szczepanik, M. Chemical characteristics of biomass ashes. *Energies* **2018**, *11*, 2885. [[CrossRef](#)]
3. Vassilev, S.V.; Baxter, D.; Andersen, L.K.; Vassileva, C.G. An overview of the composition and application of biomass ash. Part 1. Phase-mineral and chemical composition and classification. *Fuel* **2013**, *105*, 40–76. [[CrossRef](#)]
4. Chen, C.; Yu, C.; Zhang, H.; Zhai, X.; Luo, Z. Investigation on K and Cl release and migration in micro-spatial distribution during rice straw pyrolysis. *Fuel* **2016**, *167*, 180–187. [[CrossRef](#)]
5. Tchapda, A.H.; Pisupati, S.V. A review of thermal co-conversion of coal and biomass/waste. *Energies* **2014**, *7*, 1098–1148. [[CrossRef](#)]
6. Jensen, P.A.; Frandsen, F.J.; Dam-Johansen, K.; Sander, B. Experimental investigation of the transformation and release to gas phase of potassium and chlorine during straw pyrolysis. *Energy Fuels* **2000**, *14*, 1280–1285. [[CrossRef](#)]
7. Bjorkman, E.; Stromberg, B. Release of chlorine from biomass at pyrolysis and gasification conditions. *Energy Fuels* **1997**, *11*, 1026–1032. [[CrossRef](#)]
8. Knudsen, J.N.; Jensen, P.A.; Dam-Johansen, K. Transformation and release to the gas phase of Cl, K, and S during combustion of annual biomass. *Energy Fuels* **2004**, *18*, 1385–1399. [[CrossRef](#)]
9. Wang, G.; Jensen, P.A.; Wu, H.; Frandsen, F.J.; Sander, B.; Glarborg, P. Potassium capture by Kaolin, Part 1: KOH. *Energy Fuels* **2018**, *32*, 1851–1862. [[CrossRef](#)]
10. Wang, G.; Jensen, P.A.; Wu, H.; Frandsen, F.J.; Sander, B.; Glarborg, P. Potassium capture by Kaolin, Part 2: K<sub>2</sub>CO<sub>3</sub>, KCl, and K<sub>2</sub>SO<sub>4</sub>. *Energy Fuels* **2018**, *32*, 3566–3578. [[CrossRef](#)]
11. Jeong, T.; Sh, L.; Kim, J.; Lee, B.; Jeon, C. Experimental investigation of ash deposit behavior during co-combustion of bituminous coal with wood pellets and empty fruit bunches. *Energies* **2019**, *12*, 2087. [[CrossRef](#)]
12. Jin, X.; Ye, J.; Deng, L.; Che, D. Condensation behaviors of potassium during biomass combustion. *Energy Fuels* **2017**, *31*, 2951–2958. [[CrossRef](#)]
13. Niu, Y.; Zhu, Y.; Tan, H.; Hui, S.; Jing, Z.; Xu, W. Investigations on biomass slagging in utility boiler: Criterion numbers and slagging growth mechanisms. *Fuel Process. Technol.* **2014**, *128*, 499–508. [[CrossRef](#)]
14. Miles, T.R.; Miles, T.R.; Baxter, L.L.; Bryers, R.W.; Jenkins, B.M.; Oden, L.L. Boiler deposits from firing biomass fuels. *Biomass Bioenerg.* **1996**, *10*, 125–138. [[CrossRef](#)]
15. Sandberg, J.; Karlsson, C.; Fdhila, R.B. A 7 year long measurement period investigating the correlation of corrosion, deposit and fuel in a biomass fired circulated fluidized bed boiler. *Appl. Energy* **2011**, *88*, 99–110. [[CrossRef](#)]
16. Baxter, L.L.; Miles, T.R.; Miles, T.R.; Jenkins, B.M.; Milne, T.; Dayton, D.; Bryers, R.W.; Oden, L.L. The behavior of inorganic material in biomass-fired power boilers: Field and laboratory experiences. *Fuel Process. Technol.* **1998**, *54*, 47–78. [[CrossRef](#)]
17. Jensen, P.A.; Frandsen, F.J.; Hansen, J.; Dam-Johansen, K.; Henriksen, N.; Horlyck, S. SEM investigation of superheater deposits from biomass-fired boilers. *Energy Fuels* **2004**, *18*, 378–384. [[CrossRef](#)]
18. Valmari, T.; Lind, T.M.; Kauppinen, E.I.; Sfiris, G.; Nilsson, K.; Maenhaut, W. Field study on ash behavior during circulating fluidized-bed combustion of biomass. 2. Ash deposition and alkali vapor condensation. *Energy Fuels* **1999**, *13*, 390–395. [[CrossRef](#)]
19. Zhou, H.; Jensen, P.A.; Frandsen, F.J. Dynamic mechanistic model of superheater deposit growth and shedding in a biomass fired grate boiler. *Fuel* **2007**, *86*, 1519–1533. [[CrossRef](#)]
20. Tobiasen, L.; Skytte, R.; Pedersen, L.S.; Pedersen, S.T.; Lindberg, M.A. Deposit characteristic after injection of additives to a Danish straw-fired suspension boiler. *Fuel Process. Technol.* **2007**, *88*, 1108–1117. [[CrossRef](#)]

21. Zbogar, A.; Jensen, P.A.; Frandsen, F.J.; Hansen, J.; Glarborg, P. Experimental investigation of ash deposit shedding in a straw-fired boiler. *Energy Fuels* **2006**, *20*, 512–519. [[CrossRef](#)]
22. Bashir, M.S.; Jensen, P.A.; Frandsen, F.; Wedel, S.; Dam-Johansen, K.; Wadenback, J.; Pedersen, S.T. Suspension-firing of biomass. Part 1: Full-scale measurements of ash deposit build-up. *Energy Fuels* **2012**, *26*, 2317–2330. [[CrossRef](#)]
23. Madhiyanon, T.; Sathitruangsak, P.; Sungworagarn, S.; Pipatmanomai, S.; Tia, S. A pilot-scale investigation of ash and deposition formation during oil-palm empty-fruit-bunch (EFB) combustion. *Fuel Process. Technol.* **2012**, *96*, 250–264. [[CrossRef](#)]
24. Retschitzegger, S.; Gruber, T.; Brunner, T.; Obernberger, I. Short term online corrosion measurements in biomass fired boilers. Part 1: Application of a newly developed mass loss probe. *Fuel Process. Technol.* **2015**, *137*, 148–156. [[CrossRef](#)]
25. Retschitzegger, S.; Gruber, T.; Brunner, T.; Obernberger, I. Short term online corrosion measurements in biomass fired boilers. Part 2: Investigation of the corrosion behavior of three selected superheater steels for two biomass fuels. *Fuel Process. Technol.* **2016**, *142*, 59–70. [[CrossRef](#)]
26. Hansen, L.A.; Nielsen, H.P.; Frandsen, F.J.; Dam-Johansen, K.; Horlyck, S.; Karlsson, A. Influence of deposit formation on corrosion at a straw-fired boiler. *Fuel Process. Technol.* **2000**, *64*, 189–209. [[CrossRef](#)]



© 2020 by the authors. Licensee MDPI, Basel, Switzerland. This article is an open access article distributed under the terms and conditions of the Creative Commons Attribution (CC BY) license (<http://creativecommons.org/licenses/by/4.0/>).